GEOPHYSICS, VOL. 57, NO. 3 (MARCH 1992); P. 378–385, 14 FIGS.

Refractor imaging using an automated wavefront reconstruction method

David F. Aldridge* and Douglas W. Oldenburg*

ABSTRACT

The classical wavefront method for interpreting seismic refraction arrival times is implemented on a digital computer. Modern finite-difference propagation algorithms are used to downward continue recorded refraction arrival times through a near-surface heterogeneous velocity structure. Two such subsurface traveltime fields need to be reconstructed from the arrivals observed on a forward and reverse geophone spread. The locus of a shallow refracting horizon is then defined by a simple imaging condition involving the reciprocal time (the traveltime between source positions at either end of the spread). Refractor velocity is estimated in a subsequent step by calculating the directional derivative of the reconstructed subsurface wavefronts along the imaged interface. The principle limitation of the technique arises from imprecise knowledge of the overburden velocity distribution. This velocity information must be obtained from uphole times, direct and reflected arrivals, shallow refractions, and borehole data.

Analysis of synthetic data examples indicates that the technique can accurately image both synclinal and anticlinal structures. Finally, the method is tested, apparently successfully, on a shallow refraction dataset acquired at an archeological site in western Crete.

INTRODUCTION

The wavefront method is one of the earliest of the many techniques for interpreting refraction arrival times. In 1930, Thornburgh demonstrated that subsurface wavefronts could be reconstructed from surface arrival times by applying Huygens's principle in reverse. Subsequently, Hagedoorn (1959) elucidated an imaging condition for delineating a refracting horizon. First, two oppositely propagating wavefront systems are reconstructed from the arrival times recorded on a forward and reverse spread, respectively. Then, pairs of these subsurface wavefronts intersect on or slightly below the refracting interface when the sum of their times equals the known reciprocal time (the shot-to-shot traveltime). This imaging principle yields the correct spatial locus of a critically refracting horizon if the earth consists of constant velocity layers bounded by plane dipping interfaces. However, several investigators have demonstrated that the imaging condition is reasonably accurate even if the measured arrival times are due to diving rays, rather than true critically refracted rays (Hagedoorn, 1959; Rockwell, 1967; Schenck, 1967; Hill, 1987). Diving rays may arise from nonplane structure on the refracting interface, or a velocity gradient within the underlying medium.

Extensive application of the wavefront method has been limited by two factors: (1) laborious graphical techniques are required to construct the subsurface wavefront loci, and (2) detailed knowledge of the near-surface velocity structure is necessary. Our research addresses directly the first of these two issues. Instead of defining the wavefronts by a tedious graphical application of Huygens's principle (e.g., Rockwell, 1967), we use a finite-difference computer algorithm to downward continue surface arrival times through a specified velocity field. The algorithm is rapid and accurate, and is capable of handling a heterogeneous velocity structure.

Recently, Hill (1987) downward continued refracted waveforms to obtain a two-dimensional image of shallow structure. Our goal is the same, although we work with arrival times only. The advantage of this approach lies in its computational simplicity. Since the propagation algorithm operates directly in the space-time domain, no transformations of the recorded wavefield, with attendent concerns about sampling adequacy, are necessary (Clayton and McMechan, 1981; Hill, 1987). Furthermore, true amplitude recording and processing of the seismic traces are not required. However, prior picking of these traces to obtain

Presented at the 60th Annual International Meeting, Society of Exploration Geophysicists.
Manuscript received by the Editor March 26, 1991; revised manuscript received July 26, 1991.
*University of British Columbia, Department of Geophysics and Astronomy, 129-2219 Main Mall, Vancouver, B. C., Canada, V6T 1Z4.

the arrival times is necessary, and this may be a time-consuming job in some situations.

FINITE-DIFFERENCE TRAVELTIMES

Wavefront construction

Vidale (1988, 1990) has recently developed an algorithm for calculating the first arrival times of a seismic wave propagating through a two or three dimensional velocity structure. The velocity field is sampled on a uniformly spaced 2-D or 3-D grid; plane-wave finite-difference operators are used to extrapolate the traveltimes from point to point throughout this grid. Calculations are initiated at a source point within the predefined velocity field. The algorithm properly handles the various wave types that comprise first arrivals (body waves, head waves, and diffractions). Subsequent contouring of the computed traveltime field yields a visual impression of propagating wavefronts. We use the phrase *wavefront construction* to refer to traveltime loci calculated in this manner. Figure 1 depicts the subsurface wavefront systems generated by a sequence of shots buried in an earth model with undulating surface and refractor topography. The direct wave through the overburden is the initial arrival near each shot location. Beyond the crossover distance, the wave refracted by the higher velocity bedrock arrives first. The traveltimes recorded along the nonplane surface of the model are accurately computed by assigning a P-wave velocity to the uppermost layer equal to the speed of sound in air (~350 m/s). Wavefront contours are then suppressed in this region for visual clarity. The surface arrival time curves displayed in Figure 2 illustrate that nonplane topography has a complicating effect on an interpretation.

We have altered Vidale's wavefront construction algorithm in two important ways in order to improve its suitability for the shallow refraction problem. First, the traveltime calculations are initiated from a spatially extended source, rather than a point source. In the 2-D case, source activation times are specified on and inside a rectangular region located within the velocity field; arrival times at grid points outside this rectangle are generated by the normal working of the algorithm. Since wavefronts are strongly curved in the immediate vicinity of a point source, use of the plane-wave finite-difference operators will yield inaccurate traveltimes in this region. Moreover, these inaccuracies will be propagated to greater distances, where the plane wave extrapolators are locally valid. In order to avoid this problem, we calculate the near-source traveltimes via mathematically exact formulas appropriate for either a constant or linear velocity field. Although more complicated velocity distributions can be considered, these particular velocity functions provide sufficient flexibility for many traveltime computation problems.

Second, the mathematical form of the traveltime extrapolation operator is modified in those cases where there is a large velocity increase across a grid cell. This situation is relatively common in the shallow refraction environment. The interface between unconsolidated overburden and consolidated bedrock, or between saturated and unsaturated alluvium, often represents a sharp velocity increase. In these cases, as the following analysis indicates, the conventional traveltime extrapolation formula may fail.

Figure 3a depicts a system of plane wavefronts propagating across a square grid cell with side length h. We desire to calculate the arrival time at the corner numbered 4 from the known arrival times t_1, t_2, and t_3 at the other three corners of the cell. Assuming a plane wave advancing with a constant slowness s, this time is given by $t_4 = t_1 + (\sqrt{2}h \cos \theta)s$, where the angle θ describes the ray direction relative to the cell diagonal. Simple geometric analysis yields

$$\cos \theta = \sqrt{1 - \left(\frac{t_3 - t_2}{\sqrt{2}hs}\right)^2}.$$

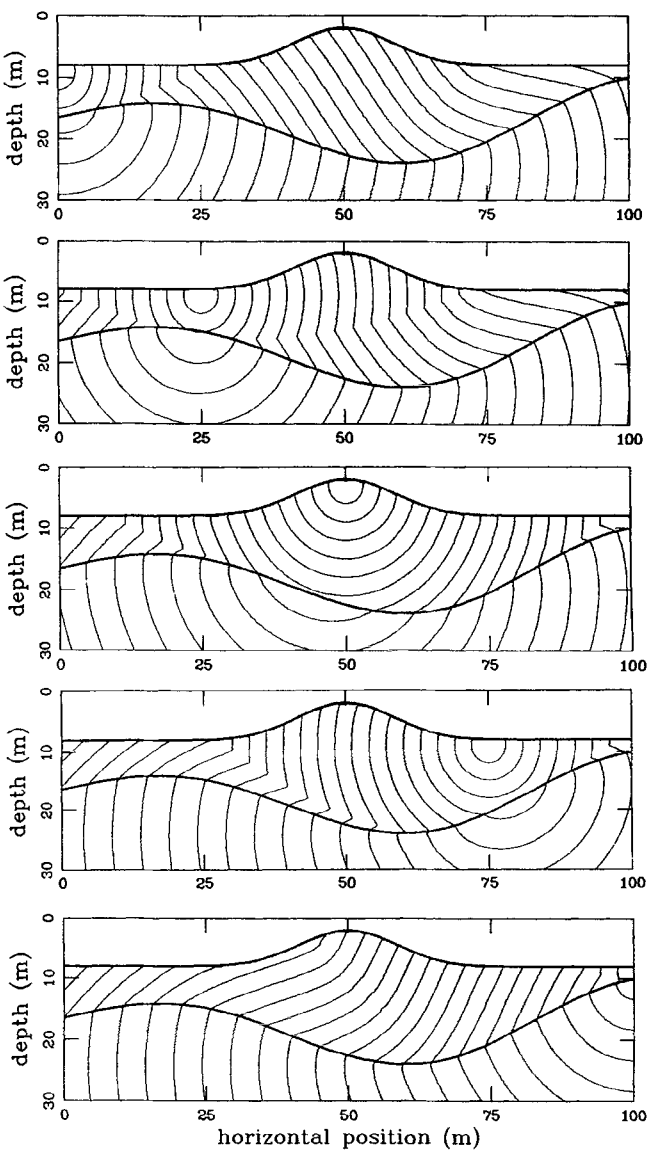

FIG. 1. Subsurface first arrival wavefronts (contour interval = 2 ms) for an earth model with undulating surface and refractor topography. Layer P-wave speeds are v_0 = 350 m/s, v_1 = 1500 m/s, and v_2 = 2500 m/s. Shots are buried 1-m deep and grid cell size is 0.2 m. For visual clarity, contours within the uppermost layer (air) are suppressed.

Hence

$$t_4 = t_1 + \sqrt{2(hs)^2 - (t_3 - t_2)^2}. \quad (1)$$

This expression is identical to Vidale's (1988) equation (3), which was derived by approximating the partial derivatives in the 2-D eikonal equation by finite differences and then solving algebraically for t_4. The present derivation clearly reveals the underlying geometric assumption of plane-wave propagation.

If the argument of the square root in equation (1) becomes negative, then the plane-wave extrapolation formula is obviously invalid. This may occur, for example, if there is a dramatic velocity increase across the cell (implying that the slowness s assigned to the cell is quite small). In these cases, we calculate the arrival time t_4 via the alternative formula

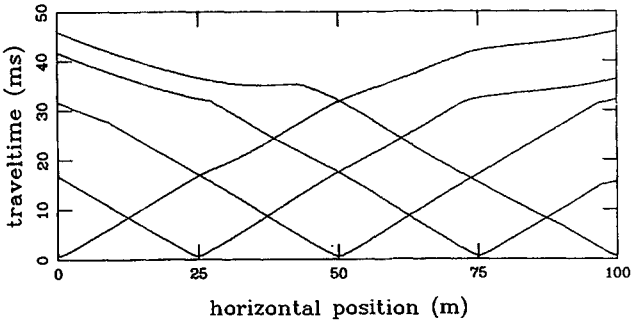

FIG. 2. Surface arrival time curves for the five wavefront systems depicted in Figure 1.

$$t_4 = \min\{t_1 + \sqrt{2}hs,\ t_2 + hs,\ t_3 + hs\}. \quad (2)$$

The geometric basis of equation (2) is illustrated in Figure 3b. In effect, we abandon the plane-wavefront approximation altogether and resort directly to Huygens's principle to calculate the next traveltime. Although this computed time is not exactly correct, extensive numerical testing indicates that equation (2) is superior to the fix advocated by Vidale (1990) (i.e., if the argument of the square root becomes negative, take $t_4 = t_1$).

Wavefront reconstruction

Figure 4 displays the forward and reverse wavefront systems generated by shooting over a shallow syncline. These are the wavefronts that give rise to the first arrival times observed on the surface. The finite-difference traveltime algorithm can now be used to recreate subsurface wavefronts from knowledge of the arrival times recorded at the surface. We place the source rectangle at zero depth and elongate it greatly in the horizontal dimension. This line source is then activated sequentially (rather than simultaneously) with an initiation function $T_S(X)$ derived from the recorded refraction arrival times $T(X)$:

$$T_S(X) = T_R - T(X), \quad (3)$$

where T_R is the reciprocal time. At source-receiver offsets X less than the crossover distance, phantom arrival times $T(X)$ can be constructed from parallel traveltime curves recorded from distant shotpoints (Rockwell, 1967; Ackermann et al., 1986). The line source generates a set of wavefronts radiating

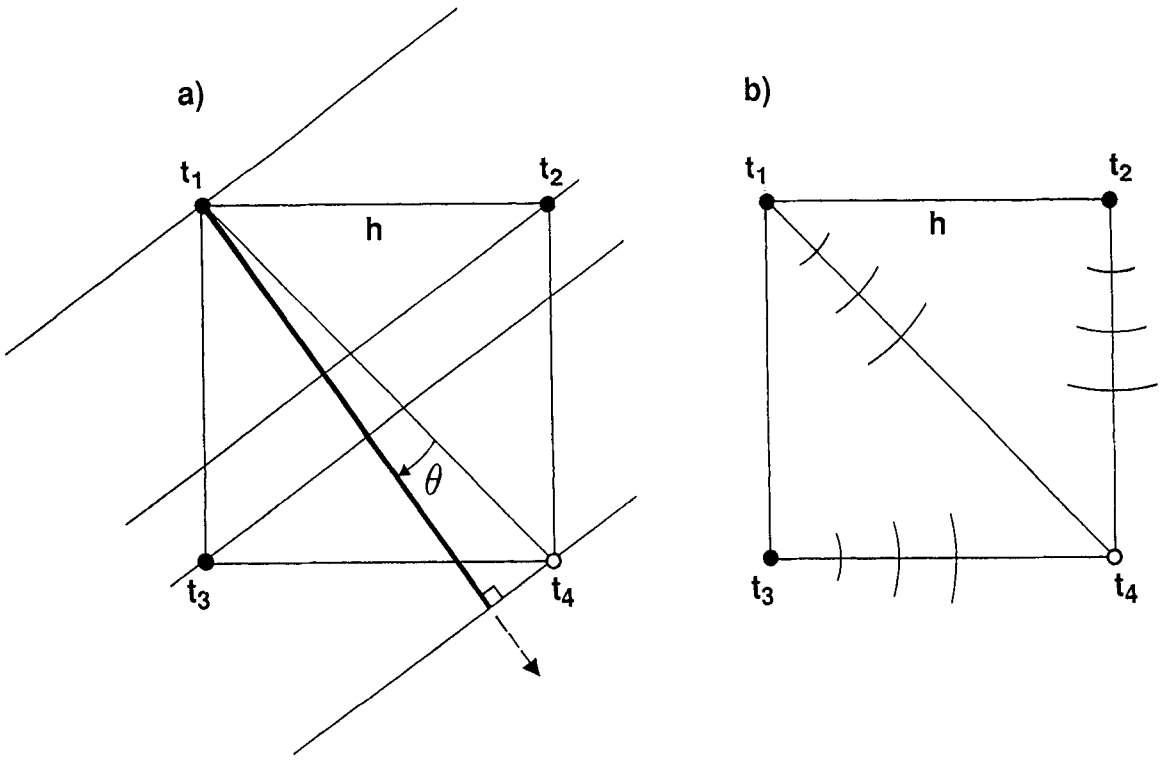

FIG. 3. Finite-difference traveltime extrapolation operators. (a) Locally plane wavefronts; θ is the angle between the ray (heavy line) and the cell diagonal. (b) Circular wavefronts. In each case, the square grid cell has side length h and assigned slowness s.

downward into the specified velocity field (Figure 5). The downward continuation velocity function $v(x, z)$ is selected as a good approximation to the actual near-surface velocity structure. Hence, within the overburden, the calculated wavefronts coincide with the emerging refracted wavefronts of Figure 4. Since the position of the refracting interface is initially unknown, the wavefronts are continued to greater depth using the known velocity field $v(x, z)$. Rockwell (1967) referred to these traveltime loci as a "directed wavefront system." We use the phrase *wavefront reconstruction* to describe the process of creating an emergent wavefront system from the recorded surface arrival times.

REFRACTOR IMAGING

Let $t_f(x, z)$ and $t_r(x, z)$ refer to the subsurface traveltime fields reconstructed from the forward and reverse arrival times, respectively. Then, according to Hagedoorn's imaging principle, the refracting interface is implicitly defined by the relation

$$t_f(x, z) + t_r(x, z) = T_R. \tag{4}$$

Figure 6 graphically illustrates the superposition of the two reconstructed wavefront systems shown in the prior figure. We systematically search the 2-D array of superposed traveltimes to locate grid points where the imaging condition (4) is satisfied. If equation (4) does not hold on a grid point, linear interpolation between adajacent points is used to find the proper depth. The resulting depth locus $z(x)$ (dashed line in Figure 6) is an accurate spatial image of the original refracting horizon, except near the edges of the input velocity field where the subsurface wavefronts are not reconstructed correctly.

Figure 7 indicates that the technique is also capable of imaging anticlinal structure. The apex of the anticline is imaged slightly too deep because the refracted rays penetrate beneath this structure, rather than propagating along the undulating interface (e.g., Hagedoorn, 1959, Figures 2 and 3). Note that a similar problem does not occur with the syncline, because there is a tendency for the diffracted ray to follow the interface in the presence of synclinal structure.

The calculated locus for the refracting horizon depends on the reciprocal time T_R and velocity field $v(x, z)$ used for downward continuation of the surface arrival times. Variations in these quantities from their correct values will induce variations in the depth and position of the refractor.

It is relatively easy to assess the dependence of the refractor image on the value of the reciprocal time. We simply add the forward and reverse subsurface traveltime fields together and contour the result for various candidate "imaging times." Figure 8a illustrates this situation for the buried syncline. If the imaging time used is less than or greater than the true reciprocal time, then the interface image is too shallow or too deep, respectively. This particular dependence upon the reciprocal time is the converse of

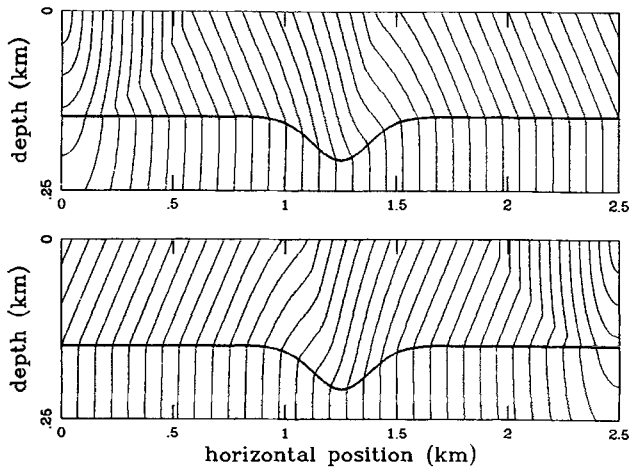

FIG. 4. Forward and reverse first arrival wavefronts for a shallow syncline model. Overburden velocity v_1 = 1500 m/s, bedrock velocity v_2 = 2500 m/s. Grid cell size is 5 m and contour interval for wavefronts is 30 ms.

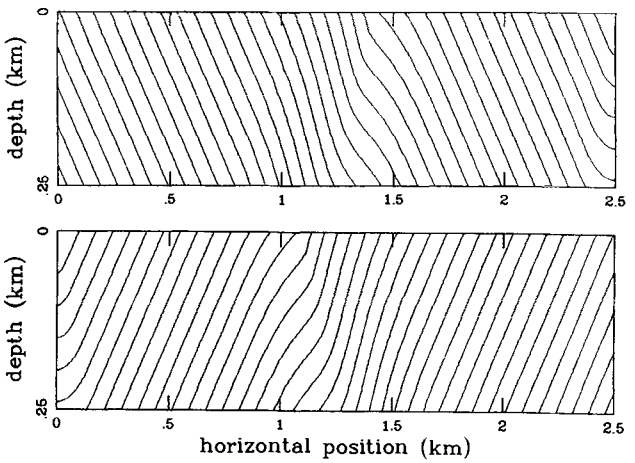

FIG. 5. Emergent wavefronts reconstructed from the surface arrival times recorded over the shallow syncline. Downward continuation velocity $v(x, z)$ = 1500 m/s. Grid cell size is 5 m and wavefront contour interval is 30 ms.

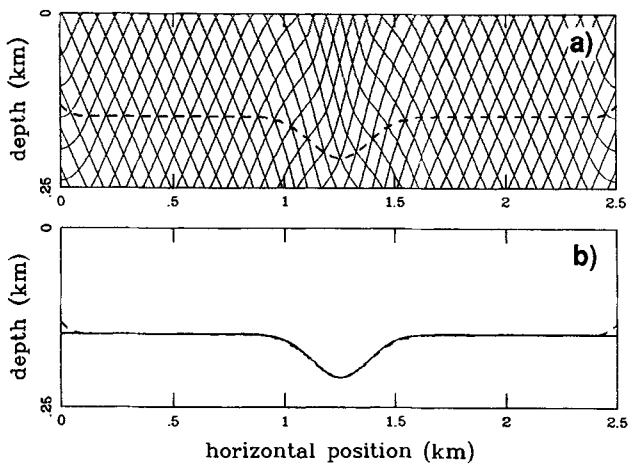

FIG. 6. (a) Superposition of the two reconstructed wavefront systems of Figure 5. Dashed line is the locus satisfying the refractor imaging condition. (b) Comparison of the true (solid) and imaged (dashed) refracting interfaces.

that predicted by the classical wavefront method (Rockwell, 1967, p. 378). The difference arises from the method of reconstructing the subsurface wavefronts. We initiate the finite-difference traveltime computations with the source function (3) and then run the algorithm forward in time. Hence, subsurface wavefronts are labeled with times *later* than the surface source values. In contrast, the classical wavefront reconstruction methods label the subsurface wavefronts with times *earlier* than the surface measured times. In either case, the true position of the interface corresponds to an imaging time equal to T_R.

Quantifying the dependence of the refractor image on the downward continuation velocity is more complicated. Forward and reverse subsurface wavefront systems must be reconstructed for each velocity function used in the analysis. Figure 8b displays a set of images of the shallow syncline calculated for various values of a constant downward continuation velocity. If the velocity is less than or greater than the actual overburden velocity, then the interface image is too shallow or too deep, respectively. Moreover, a grossly incorrect continuation velocity distorts the shape of the interface structure. Hence, in common with many other seismic refraction interpretation techniques, accurate time-to-depth conversion with the wavefront method requires good knowledge of the overburden velocity distribution. This information can be obtained from uphole times, direct and reflected arrivals, shallow refractions, and borehole data.

Finally, the accuracy of the solution depends on the reliability of the picked first arrival times. The ability of the method to resolve small scale features on the refracting horizon is also limited by the field geophone interval. These phenomena are analyzed by performing the inversion with noisy traveltime data sampled at an assumed geophone interval. Figure 9 displays the refractor image obtained by downward continuing error contaminated arrival times sampled every 25 m. We added spatially correlated, normally distributed time errors (standard deviation = 5 ms; correlation distance = 100 m) to the theoretically exact refraction picks. A cubic spline is then loosely fitted to the noisy arrival times and is used in equation (3) for the source initiation function. The experiment has detected the presence of the syncline, and its lateral position and depth are approximately correct. Long wavelength undulations on the refractor are artifacts of the spatially correlated noise, but are not unduly harmful to the structural interpretation.

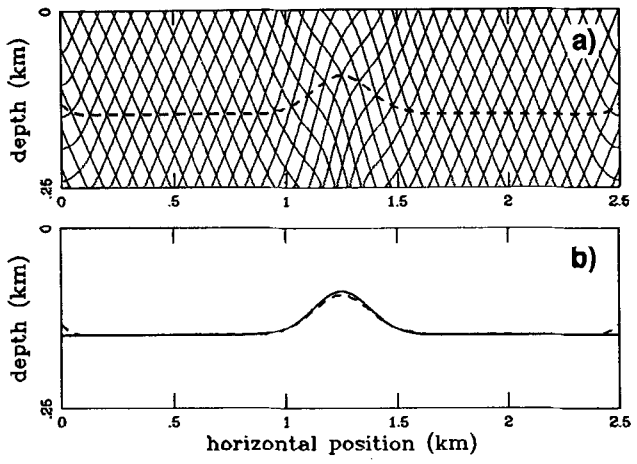

FIG. 7. (a) Superposition of the forward and reverse reconstructed wavefronts (contour interval = 30 msec) over a shallow anticline. Dashed line is the refractor image. (b) Comparison of the true (solid) and imaged (dashed) refracting interfaces.

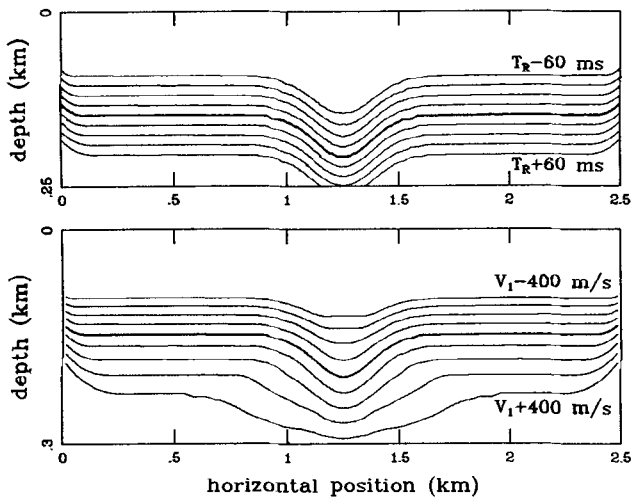

FIG. 8. Dependence of the syncline locus on imaging time (top) and downward continuation velocity (bottom). Different images correspond to increments of 10 ms in imaging time and 100 m/s in velocity, respectively. Heavy lines are the images corresponding to the correct values of T_R and v.

REFRACTOR VELOCITY ESTIMATION

A particular advantage of the wavefront method is that the interface depth calculation is independent of the refractor velocity. Rather, the velocity of the substratum can be estimated after the position of the refracting horizon is determined. The distance between two points on the interface divided by the difference in the reconstructed wavefront times at these points is an estimate of the refractor velocity. This value is assigned to the midpoint of the two points for plotting purposes. In effect, the directional derivative of the subsurface traveltime field along the interface locus is computed by a centered finite-difference formula; the reciprocal

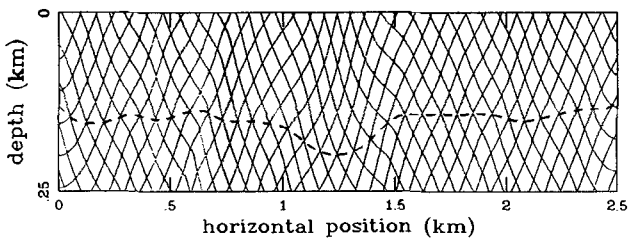

FIG. 9. Reconstructed wavefronts and syncline image formed from noisy traveltime data sampled at a geophone interval of 25 m. Grid cell size is 5 m and wavefront contour interval is 30 ms. Long wavelength undulations on the refractor arise from spatially correlated traveltime errors.

of this value corresponds to the local velocity of the refractor. Either the forward or reverse wavefront systems may be used for the computation. Figure 10 illustrates that the refractor velocity estimated in this manner possesses systematic errors related to the interface structure. However, for the two synthetic examples examined here, the inferred velocity values are everywhere within 3 percent (or ±75 m/s) of the correct values.

FIELD DATA EXAMPLE

We have tested the interface imaging procedure with a shallow refraction dataset acquired at the archeological site of Phalasarna in western Crete. Hadjidaki (1988) discusses the historical and archeological significance of this site and also gives a detailed description of the surface and near subsurface conditions. Forward and reverse refraction profiles were recorded along an inline spread of 18 geophones (geophone interval = .5 m, near source offset = .5 m) during the summer of 1989. The data acquisition system consisted of a portable signal stacking seismograph with a hammer energy source. First arrival time picks were made on stacked traces in order to reduce random errors induced by noise.

The arrival times observed at reciprocal source positions at opposite ends of the spread differ slightly (16.40 ms versus 16.70 ms on the forward and reverse profiles, respectively). Since a successful inversion requires consistency in the measured reciprocal times, we apply reciprocal time corrections (Hatherly, 1982) to the picked arrival times. A constant time shift is added to the raw time picks on each source gather in order to adjust the observed reciprocal times to the average value of 16.55 ms.

Figure 11 displays the 18 first break picks recorded on the forward and reverse profiles after application of these reciprocal time corrections. A preliminary interpretation of the plotted traveltime curves identifies the direct and refracted branches. Overburden velocity, determined from the slopes of the direct arrival segments, exhibits a weak lateral variation (~8 percent) over the 9-m spread length. We use this information to construct a near-surface velocity function for subsequent downward continuation of the refracted arrival times. A cubic spline is fitted to the 16 refraction picks on each spread and is extrapolated to zero offset as a straight line. These curves are then used in equation (3) to calculate the source initiation functions required for the wavefront reconstruction algorithm.

Figure 12a depicts the subsurface wavefronts generated by downward continuing the refracted arrival times through a near-surface velocity field given by $v(x) = 252 - 2.11x$ (x in m and v in m/s). A shallow undulating interface is then imaged using the corrected reciprocal time $T_R = 16.55$ ms. The refractor velocity estimate (Figure 12b) exhibits two distinct zones: (1) abrupt variations about 800 m/s on the left, and (2) a low-velocity zone slower than 800 m/s on the right.

We test the validity of various refractor velocity functions by using the wavefront construction algorithm to compare predicted traveltimes with the observed traveltimes. A uniform refractor velocity of 800 m/s leads to unacceptably

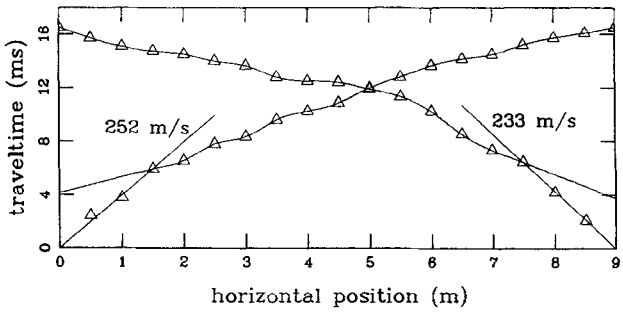

FIG. 11. Shallow refraction traveltime data acquired at the dry harbor of Phalasarna, Crete. First break picks are indicated by triangles, and interpreted arrival time branches by smooth curves.

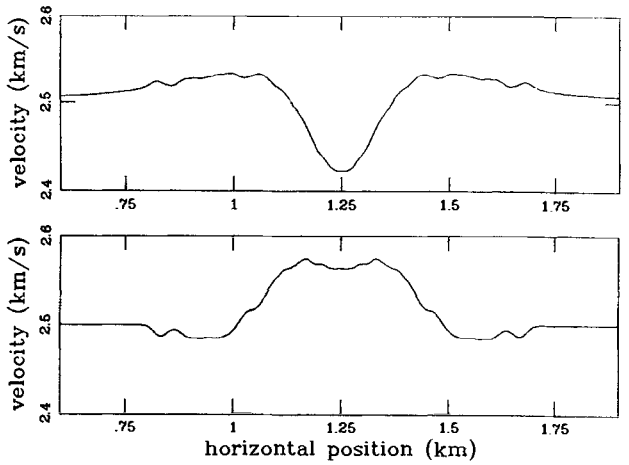

FIG. 10. Refractor velocity estimates for the syncline (top) and anticline (bottom) models. The spatial differencing interval used for the calculation is 200 m. Small amplitude, short wavelength oscillations are artifacts of the grid interval.

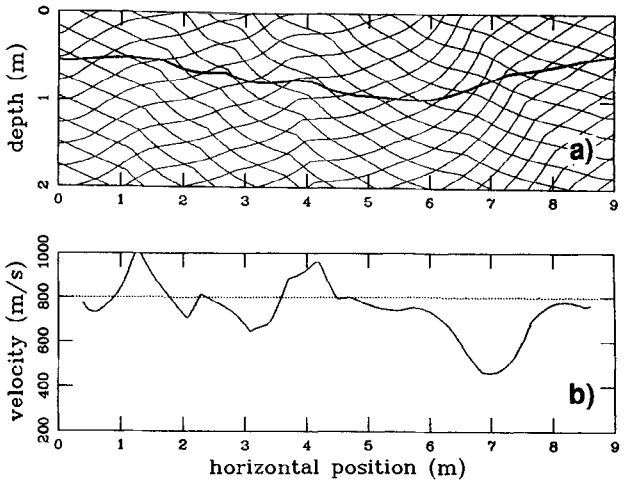

FIG. 12. (a) Forward and reverse subsurface wavefronts (contour interval = 1 ms) reconstructed by downward continuing the refracted arrival times of Figure 11. Grid cell size is 0.02 m. Heavy line is the refractor image. (b) Refractor velocity function (solid curve) calculated with a differencing interval of 0.8 m.

large differences (Figure 13b). When a low-velocity zone is introduced into the refractor, good agreement is obtained (Figure 13c). The effect of the low velocity zone is evident in the plotted forward and reverse wavefronts of Figure 14 between 6 and 8 m horizontal position. Note that the strong variations in refractor velocity displayed on the left in Figure 12b need not be incorporated into the model to obtain an adequate fit to the measured arrival times. Further adjustment of the refractor velocity to obtain a closer fit is probably unwarranted.

Although the recovered model of Figure 14 generates acceptable predicted traveltimes, we cannot state with certainty that this is the correct earth model. Other interpretations of the observed traveltime data, incorporating multiple layers or lateral changes in structure and/or velocity, are possible. Since the refraction dataset does not include arrival times recorded from far offset shotpoints, it is not possible to distinguish between these alternatives (Ackermann et al., 1986). However, the inferred model is consistent with known subsurface information from the vicinity of the refraction profile. Archeological trenching conducted about 17 m distant encountered dipping sandstone bedrock at approximately 1.8 m depth (Hadjidaki, 1988). Various earthen and gravel layers overlie the bedrock. We think that a porous, aerated sandstone can have a P-wave velocity as low as ~800 m/s. Hence, our preliminary interpretation is that the interface imaged in Figure 14 is the upper surface of the sandstone bedrock. The very low velocity between 6 and 8 m may be a zone of more extensive weathering, fracturing, or aeration. Alternately, it is possible that we have imaged one of the overlying shallow gravel layers.

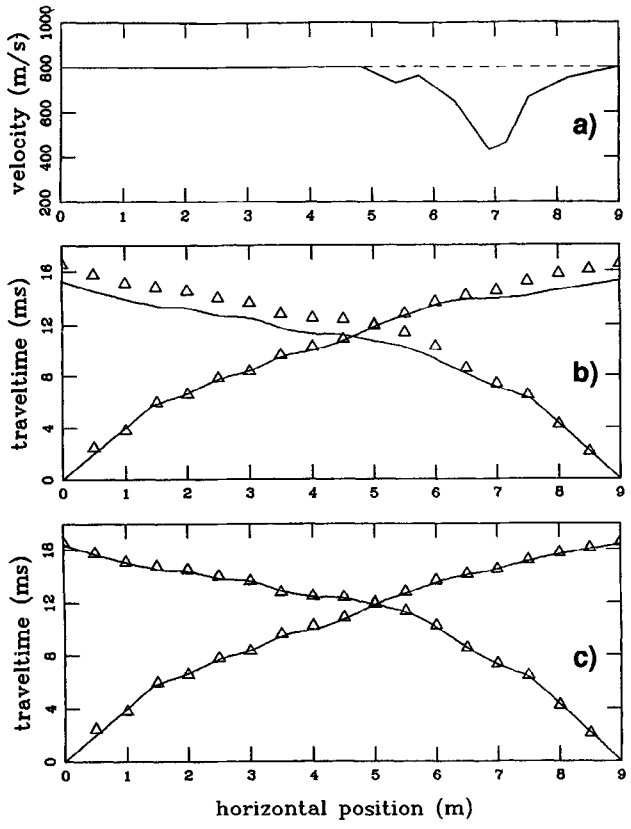

FIG. 13. Comparison of observed and predicted first-break times for two refractor velocity functions. (a) Constant velocity (dashed) equals 800 m/s and variable velocity (solid) includes a low velocity zone between 6 and 8 m. (b) Predicted traveltimes calculated with the constant refractor velocity. (c) Predicted traveltimes calculated with the variable refractor velocity.

CONCLUSIONS

The essential requirements for reconstructing shallow refracted wavefronts are:

1) arrival times $T(X)$ from a given marker horizon recorded (or phantomed) on a forward and reverse spread,
2) a reciprocal time T_R,
3) a near-surface velocity function $v(x, z)$.

A simple modification of Vidale's finite-difference traveltime algorithm then allows the rapid calculation of the subsurface wavefront systems that give rise to the recorded arrival times. Although our synthetic examples use a constant near-surface velocity, downward continuation through a varying velocity field is also possible with no increase in computation time. The buried refracting horizon is delineated in a subsequent step by applying Hagedoorn's imaging principle. No prior assumption regarding the refractor velocity is required. Rather, the velocity of the substratum can be estimated by calculating the directional derivative of the reconstructed wavefront systems along the imaged interface.

Picking of first arrival times and assignment of these picks to specific refractors are necessary in this method. The final locus for the refracting interface is sensitive to errors in the picked times, as well as to an incorrect choice of the reciprocal time and velocity field. However, since the technique is not computationally intensive, it is possible to assess the magnitude of the position and depth uncertainty by performing the inversion repetitively. The forward modeling capabilities of the finite-difference traveltime algorithm can also be used to quickly generate predicted arrival times

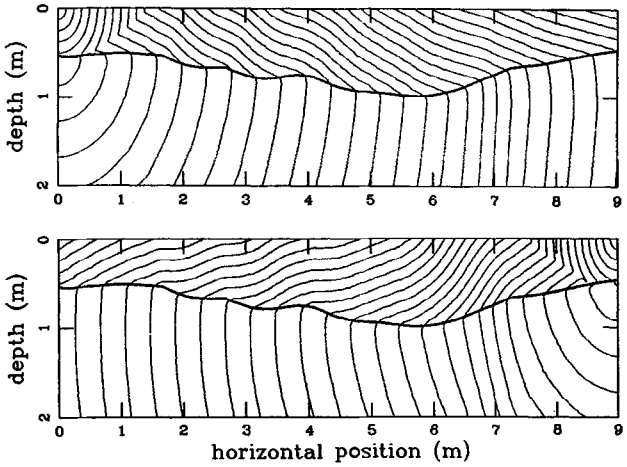

FIG. 14. Subsurface wavefronts (contour interval = 0.5 ms) constructed from the earth model with the laterally varying refractor velocity. Grid cell size is 0.02 m. Note the effect of the low-velocity zone between 6 and 8 m.

from the inferred subsurface model. Comparison of these times with the observed data is a powerful method of establishing the significance of various features of the recovered earth model.

Finally, we have identified two specific problem areas with the automated wavefront reconstruction method that merit further research: (1) downward continuation of traveltimes recorded along a nonplane surface, and (2) correction of the refractor velocity function for the effects of structurally induced errors. Although a fully automated solution to these problems is not yet available, this should not prevent the immediate application of the method in shallow seismic refraction exploration.

ACKNOWLEDGMENTS

This research was supported by NSERC operating grant 5-84270, a *University Research Grant from Imperial Oil Ltd.*, and a Killam predoctoral fellowship from the University of British Columbia. The shallow refraction data set from Phalasarna, Crete was acquired during the summer of 1989 by Guy Cross, of the Department of Geophysics and Astronomy at UBC.

REFERENCES

Ackermann, H. D., Pankratz, L. W., and Dansereau, D., 1986, Resolution of ambiguities of seismic refraction traveltime curves: Geophysics, **51**, 223–235.

Clayton, R. W., and McMechan, G. A., 1981, Inversion of refraction data by wavefield continuation: Geophysics, **46**, 860–868.

Hadjidaki, E., 1988, Preliminary report of excavations at the harbor of Phalasarna in West Crete: Am. Jour. Archaeol., **92**, 463–479.

Hagedoorn, J. G., 1959, The plus-minus method of interpreting seismic refraction sections: Geophys. Prosp., **7**, 158–182.

Hatherly, P. J., 1982, A computer method for determining seismic first arrival times: Geophysics, **47**, 1431–1436.

Hill, N. R., 1987, Downward continuation of refracted arrivals to determine shallow structure: Geophysics, **52**, 1188–1198.

Rockwell, D. W., 1967, A general wavefront method, *in* Musgrave, A. W., Ed., Seismic refraction prospecting: Soc. Expl. Geophys., 363–415.

Schenk, F. L., 1967, Refraction solutions and wavefront targeting, *in* Musgrave, A. W., Ed., Seismic refraction prospecting: Soc. Expl. Geophys., 416–425.

Thornburgh, H. R., 1930, Wave-front diagrams in seismic interpretation: AAPG Bull., **14**, 185–200.

Vidale, J., 1988, Finite-difference calculation of travel times: Bull., Seis. Soc. Am., **78**, 2062–2076.

——— 1990, Finite-difference calculation of traveltimes in three dimensions: Geophysics, **55**, 521–526.